Cassini-Plasma Interaction Simulations Revealing the Cassini Ion Wake Characteristics: Implications for In-Situ Data Analyses and Ion Temperature Estimates

M. Holmberg, F. Cipriani, T. Nilsson, S. Hess, H. Huybrighs, L. Z. Hadid, G. Déprez, R. Wilson, M. Morooka, M. Felici

JGR Space Physics

RESEARCH ARTICLE
10.1029/2020JA029026

Key Points:

- The Cassini ion wake is characterized and it is demonstrated that the ion wake can have a substantial impact on the Cassini LP measurements
- Our study indicates that earlier estimates of the ion temperature in the inner magnetosphere of Saturn are overestimated
- The software SPIS provides accurate simulation results for typical magnetospheric conditions

Supporting Information:

Supporting Information may be found in the online version of this article.

Correspondence to:

M. K. G. Holmberg,
mika.holmberg@pm.me

Citation:

Holmberg, M. K. G., Cipriani, F., Nilsson, T., Hess, S., Huybrighs, H. L. F., Hadid, L. Z., et al. (2021). Cassini-plasma interaction simulations revealing the Cassini ion wake characteristics: Implications for in-situ data analyses and ion temperature estimates. *Journal of Geophysical Research: Space Physics*, *126*, e2020JA029026. https://doi.org/10.1029/2020JA029026

Received 18 DEC 2020
Accepted 18 JUN 2021

Cassini-Plasma Interaction Simulations Revealing the Cassini Ion Wake Characteristics: Implications for In-Situ Data Analyses and Ion Temperature Estimates

M. K. G. Holmberg[1], F. Cipriani[1], T. Nilsson[2], S. Hess[3], H. L. F. Huybrighs[1], L. Z. Hadid[1,4], G. Déprez[1], R. J. Wilson[5], M. W. Morooka[2], and M. Felici[6]

[1]European Space Research and Technology Center, European Space Agency, Noordwijk, The Netherlands, [2]Swedish Institute of Space Physics, Uppsala, Sweden, [3]DESP - Space Environment Department, ONERA, Toulouse, France, [4]LPP, CNRS, École Polytechnique, Sorbonne Université, Observatoire de Paris, Université Paris-Saclay, Palaiseau, Paris, France, [5]Laboratory for Atmospheric and Space Physics, University of Colorado Boulder, Boulder, CO, USA, [6]Center for Space Physics, Boston University, Boston, MA, USA

Abstract We have used Spacecraft Plasma Interaction Software (SPIS) simulations to study the characteristics (i.e., dimensions, ion depletion, and evolution with the changing spacecraft attitude) of the Cassini ion wake. We focus on two regions, the plasma disk at 4.5–4.7 R_S, where the most prominent wake structure will be formed, and at 7.6 R_S, close to the maximum distance at which a wake structure can be detected in the Cassini Langmuir probe (LP) data. This study also reveals how the ion wake and the spacecraft plasma interaction have impacted the Cassini LP measurements in the studied environments, for example, with a strong decrease in the measured ion density but with minor interference from the photoelectrons and secondary electrons originating from the spacecraft. The simulated ion densities and spacecraft potentials are in very good agreement with the LP measurements. This shows that SPIS is an excellent tool to use for analyses of LP data, when spacecraft material properties and environmental parameters are known and used correctly. The simulation results are also used to put constraints on the ion temperature estimates in the inner magnetosphere of Saturn. The best agreement between the simulated and measured ion density is obtained using an ion temperature of 8 eV at ~4.6 R_S. This study also shows that SPIS simulations can be used in order to better constrain plasma parameters in regions where accurate measurements are not available.

1. Introduction

All scientific space missions encounter the problems of spacecraft interferences on measurements, to varying degrees. Occasionally the disturbances are so severe that they make it difficult to analyze the desired measurements and in extreme cases such interferences can incorrectly be interpreted as actual phenomena occurring in the studied system. It is therefore paramount that the disturbing effect of the spacecraft is correctly analyzed and characterized.

One important perturbation caused by the spacecraft is the ion wake formation that occurs when the relative speed of a spacecraft exceeds the ion thermal speed of the surrounding plasma. Commonly the relative speed of the spacecraft is supersonic with respect to the ions but subsonic with respect to the electrons, which means that the electrons will be able to fill up the wake but the ions will not. The ion wake structure is difficult to study analytically but can be well understood with the use of numerical models. In this study we investigate the ion wake of the Cassini spacecraft using the Spacecraft Plasma Interaction Software (SPIS) version 6.0.4. The formation of an ion wake behind Cassini was briefly discussed by Holmberg et al. (2017), who also showed that the ion wake can have a substantial impact on the ambient plasma measurements resulting in an underestimation of the ion density with up to one order of magnitude. In earlier studies, the plasma measurements recorded in the ion wake of Cassini have either been excluded from the study (e.g., in Holmberg et al., 2017; Morooka et al., 2018, 2019; Hadid et al., 2019) or ignored, when the impact of the ion wake measurements has been negligible (e.g., in Wahlund et al., 2005; Holmberg et al., 2012). For this study we will use the LP ion density measurements in the Cassini ion wake compared with SPIS ion wake simulations in order to better understand the LP measurements, but also to verify the accuracy of such simulation results. A good agreement between measured and simulated parameters serves

as a confirmation that SPIS simulations will produce realistic and accurate results in environments similar to the ones used in this study. This is of importance not only for the analysis of spacecraft measurements but also for preparatory studies for future missions, such as JUICE and Europa Clipper.

SPIS is an open-source simulation software used for modeling the interaction between the spacecraft and the surrounding plasma environment. It was initiated in 2001 by the European Space Agency (ESA), supported by the National Center for Space Studies (CNES), and developed in collaboration with the French Aerospace Laboratory (ONERA) and Artenum. SPIS is a Java based hybrid code package that can handle both a kinetic treatment of the particle populations, using a Particle-In-Cell (PIC) method, and a fluid treatment. The simulation set-up includes defining the spacecraft geometry, computational mesh, spacecraft material properties, internal circuitry, and the simulated environment. A description of SPIS and its modeling capabilities can be found in Sarrailh et al. (2015).

SPIS has previously been used for similar projects, such as simulating the ion wake of Rosetta in the solar wind (Sjögren et al., 2012) or the Parker Solar Probe and Solar Orbiter (Guillemant et al., 2013), but simulation results have rarely been compared with in-situ measurements. Engwall et al. (2006) used PicUp3D, a predecessor of SPIS, to simulate ion wake disturbances on the Cluster spacecraft. They showed a good agreement between the simulated electric field and measured spacecraft wake-induced electric field variations for Cluster. Engwall et al. (2006) also showed that for a positively charged spacecraft with a spacecraft potential larger than the ion flow and thermal energies, the size of the ion wake will not be decided by the physical structure of the spacecraft but by the equipotential surface around the spacecraft. For an illustration of ions being deflected by a strongly positively charged spacecraft and forming an enhanced ion wake structure see Engwall et al. (2006) their Figure 1.

Miloch et al. (2012) studied the ion wake formation behind Cassini using the 2D and 3D PIC codes DiP2D and DiP3D. They concluded that the shape of the wake structure might be different depending on the ion species involved. Lighter ions may experience ion focusing which will cause the ion density behind the wake to exceed the ambient ion density.

2. Simulation Set-Up

2.1. Cassini and Its Instruments

The Cassini - Huygens mission was a joint mission between NASA, ESA, and the Italian Space Agency (ASI). The spacecraft was launched in 1997 and went into orbit around Saturn in 2004. The mission was terminated in 2017 when the spacecraft was deliberately plunged into Saturn in order to avoid potential biological contamination of Saturn's moons. Cassini - Huygens held 18 instrument packages in total whereof one was the Radio and Plasma Wave Science (RPWS). The RPWS consisted of one Langmuir probe (LP), three nearly orthogonal 10-m electric field antennas, and three orthogonal search coil magnetometers. RPWS was used to measure radio emissions, plasma waves, thermal plasma, and dust in the space environment of Saturn.

In order to perform the SPIS simulations, we first need to define the spacecraft geometry. For the sake of simplicity, the spacecraft dimensions have been extracted from a detailed 3D model provided by the Jet Propulsion Laboratory (JPL) and the obtained dimensions have been compared to the blue prints of Cassini. Three images of Cassini are shown in Figure 1. Figure 1a shows the actual spacecraft prior to launch, Figure 1b shows the Blender 3D model, and Figure 1c shows the simplified spacecraft model used in this study. The SPIS Cassini model includes the spacecraft body, the high-gain antenna (HGA), the magnetometer (MAG) boom, the LP without the boom, and the fields and particles pallet that held the Cassini Plasma Spectrometer (CAPS), the Magnetospheric Imaging Instrument (MIMI) and the Ion and Neutral Mass Spectrometer (INMS). The inclusion or exclusion of the various spacecraft parts have been carefully considered with the aim of saving simulation time without losing accuracy. For example, the Cassini model does not include the devices and structures located in between the HGA and the spacecraft body, since including these structures had an insignificant impact on the final simulation results but resulted in longer simulation times, which is further discussed in Section 3.3.

In addition to the spacecraft geometry we also need to know the spacecraft materials. The SPIS material library contains a number of different materials commonly used for space applications. The library lists the

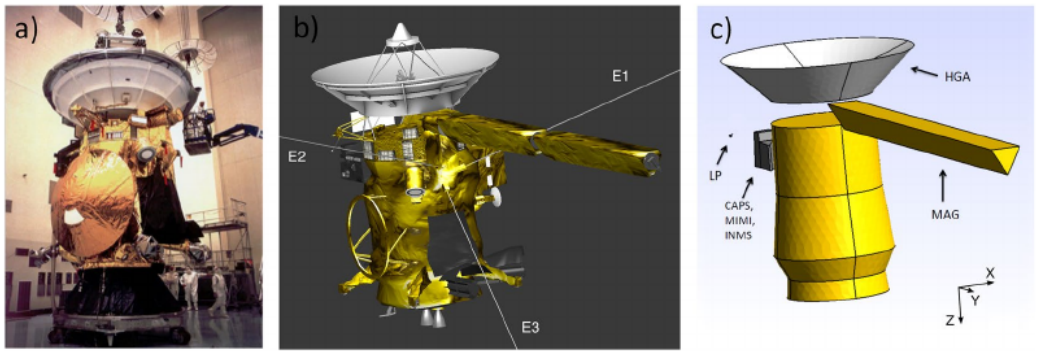

Figure 1. (a) The Cassini spacecraft prior to launch (image credit NASA/JPL-Caltech). (b) The detailed 3D model of Cassini, including the Radio and Plasma Wave Science (RPWS) electric field antennas, marked E1 to E3. (c) The simplified Cassini spacecraft model suitable for Spacecraft Plasma Interaction Software (SPIS) simulations. Panel (a) also shows the Huygens probe, the large golden dish attached to the side of the spacecraft, which was released soon after the orbit insertion and therefore excluded from the SPIS model.

material properties needed for spacecraft - plasma interaction simulations. This includes the photoelectron and secondary electron emission yield, which gives the probability of an electron being emitted from the material as a function of the energy of the incoming radiation or particle. The impact on the final simulation results from photoelectron and secondary electron emissions is discussed in Section 3.2.

The spacecraft body was modeled as a 3.64 m high cylinder with a varying radius where $r_{min} = 1$ m and $r_{max} = 1.26$ m. The shape of the actual spacecraft is bulky and irregular, which has been approximated by varying the radius of the cylinder shape by using the average radius for cross-sections at five different positions in $Z_{s/c}$. The spacecraft body is covered with Multi-layer insulation (MLI) blankets in black kapton (Lin et al., 1995) used for thermal insulation. Black kapton is commonly used as MLI so the material properties are readily available in the SPIS material library. The HGA is approximated as a dish with a height of 0.11 m and $r_{min,HGA} = 1.08$ m and $r_{max,HGA} = 2$ m. The HGA is covered with the white silicone paint PCBZ. The MAG boom is 9.66 m long and covered in black kapton. All the different parts of the spacecraft have been simulated as one electrical node, meaning that they are connected to spacecraft ground.

In addition, our SPIS Cassini model also includes the field and particle pallet that held the CAPS, MIMI, and INMS instruments, see Figure 1c. This structure was included since it is located relatively close to the Langmuir probe, however, the simulations showed its importance for the ion wake formation to be small. The instruments and the pallet is covered in black kapton. The LP, with Ti material properties, has been included in a few simulations. Due to the small surface area of the LP its impact on the wake formation and the surface potential of the spacecraft is negligible. Its small size also results in more demanding simulations. Hence, the LP has been excluded from the majority of the simulations presented in this study. The dimensions and position of the LP have been obtained from the original blue prints.

The presented simulations use the Cassini spacecraft coordinate system, shown in Figure 1c, which is defined as:

1. $X_{s/c}$ completes the right handed set after $Y_{s/c}$ and $Z_{s/c}$ are defined
2. $Y_{s/c}$ is in the MAG boom direction
3. $Z_{s/c}$ is in the opposite direction of the HGA

The top part of the spacecraft body, excluding the HGA, is the Upper Equipment Module (UEM). The level $Z_{s/c} = 0$ is found 473 mm below the top of the UEM. The position of the center of the LP sphere, in the spacecraft coordinate system, is at $(-2.288, 0.663, -0.489)$ m. This position is derived from blueprints of the spacecraft and of the Langmuir probe.

For the environment parameters of the presented simulations we have used measurements from the Cassini instruments presented below. The RPWS Langmuir probe is a spherical probe, 5 cm in diameter and made of Ti with a TiN coating. The sphere was mounted on a 0.8 m long boom on top of a tripod mounting, giving

the probe a distance of approximately 1.5 m from the nearest spacecraft surface. The Cassini LP was used to measure electron density (down to around 0.001 cm^{-3}), ion density (down to around 1 cm^{-3}), electron and ion temperatures, and ion velocity. The location of the probe is shown in Figures 1c and 1b. The probe is not visible in Figure 1a because it was stowed in preparation for launch.

We also used electron densities obtained from the RPWS electric field antenna measurements of upper hybrid emissions. The frequency of upper hybrid emissions depends on the magnetic field strength and the electron density. Hence, electron densities down to around 0.5 cm^{-3} can be obtained from the RPWS electric field antenna measurements in combination with the measured magnetic field strength. The RPWS electric field antennas are shown in Figure 1b, marked E1 to E3. A full description of the RPWS instrument package can be found in Gurnett et al. (2004).

The Cassini Plasma Spectrometer (CAPS) measured plasma density, temperature, and ion velocity. CAPS consisted of three sensors, all using charged particle motions in electric fields to study the surrounding plasma. The Electron Spectrometer (ELS) measured electrons with energies ranging from 0.7 eV to 30 keV, and the Ion Beam Spectrometer (IBS) and Ion Mass Spectrometer (IMS) measured positive ions in the energy ranges 1 eV–50 keV. The location of CAPS is shown in Figure 1c. A full description of CAPS is given by Young et al. (2004). Two different methods are used to obtain the ion density, velocity, and temperature, from the IMS measurements. The two methods are explained in detail in Wilson et al. (2017) and are referred to as LANL and LASP after the two institutes where they were developed. We have used the results from both methods whenever available.

2.2. The Studied Time Intervals

In order to compare the SPIS ion wake simulation results with the LP ion density measurements, two time intervals were chosen. The two cases were chosen based only on the conditions that a decrease in ion density could easily be detected as the LP moved into the wake and that more than two measurements were performed within the wake. No other conditions were used, in order not to affect the correlation between the simulated and measured ion densities. It is important to point out that the second condition is the most restricting condition since most of the wake encounters are over short time intervals that will only be covered by one or two data points.

The time interval 2010-03-03 10:10 to 11:00, with radial distances between 4.5 and 4.8 R_S, was chosen to characterize a strong ion wake signature and will be presented in detail. This time interval, and any given time within this time interval, will be referred to as Case 1. The time interval 2005-12-24 10:55 to 11:55, with radial distances between 7.3 and 7.8 R_S, was chosen to show the weak ion wake signature that is found farther out in the magnetosphere and will be briefly discussed. This time interval, and any give time within this time interval, will be referred to as Case 2. The orbital trajectories for the two cases are presented in Figure 2. The figure gives the trajectory projection onto the xz- and xy-planes in the Saturn Solar Equatorial (SSQ) coordinate system. The SSQ coordinate system is defined as:

1. X_{SSQ} is given by the cross product of Y_{SSQ} and Z_{SSQ}
2. Y_{SSQ} is given by the cross product of Z_{SSQ} and the Saturn-Sun vector
3. Z_{SSQ} is aligned with the spin axis of Saturn

The orbit segments of the studied time intervals are marked in red (2010-03-03 10:10 to 11:00) and blue (2005-12-24 10:55 to 11:55) in Figure 2.

2.3. The Spacecraft Attitude and Environment of Case 1

In order to perform the SPIS simulations we also need an accurate description of the environment that the spacecraft is located in. To build this environment we cannot use disturbed measurements but have to rely on a combination of the LP measurements performed before and after the ion wake encounters, results from earlier statistical studies of LP measurements from the same magnetospheric regions, and undisturbed measurements from the other Cassini instruments, such as CAPS, MAG, and the RPWS electric field antennas. This Section gives a description of how the simulation environments are defined.

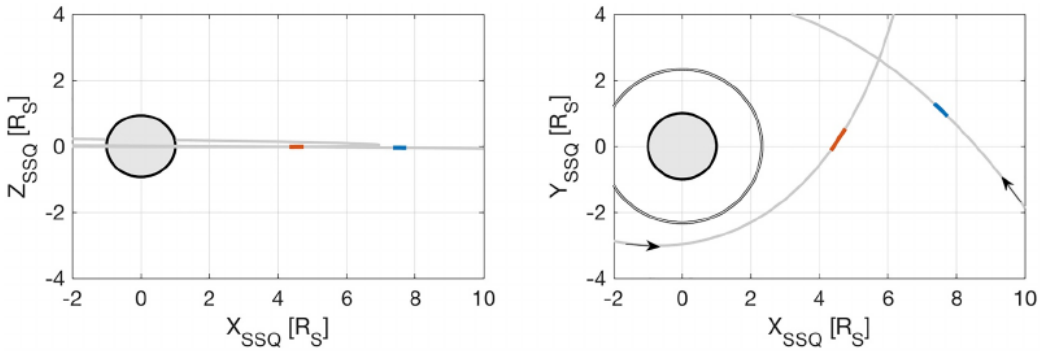

Figure 2. The Cassini trajectories in Saturn Solar Equatorial coordinates for the studied time intervals 2010-03-03 10:10 to 11:00 (red) and 2005-12-24 10:55 to 11:55 (blue). The extensions of the orbits are given in gray. The middle circle illustrates Saturn. One of the outer rings, the *F* ring, is included as a reference (gray circle with radius $r_F \approx 2.3\ R_S$).

We have performed five different simulations for the time interval 2010-03-03 10:10 to 11:00, Case 1, in order to reproduce the ion wake encounter accurately. Figure 3 illustrates the rolling of the spacecraft during the studied time interval. The five simulations represent the following situations:

1. At 10:29, just before the ion wake encounter when the LP is still measuring the undisturbed plasma, the angle between the flow direction and the LP is close to 90°. Marked as (1) in Figure 3
2. At 10:33, the LP has entered the wake region, the angle is close to 45°
3. At 10:39, the LP is in the middle of the wake, this is where the lowest ion density is measured. Marked as (3) in Figure 3
4. At 10:43, the LP is moving out of the wake region, the angle is close to 45°
5. At 10:50, the LP is again measuring the undisturbed plasma after the wake encounter. The angle between the flow direction and the LP is close to 90°. Marked as (5) in Figure 3

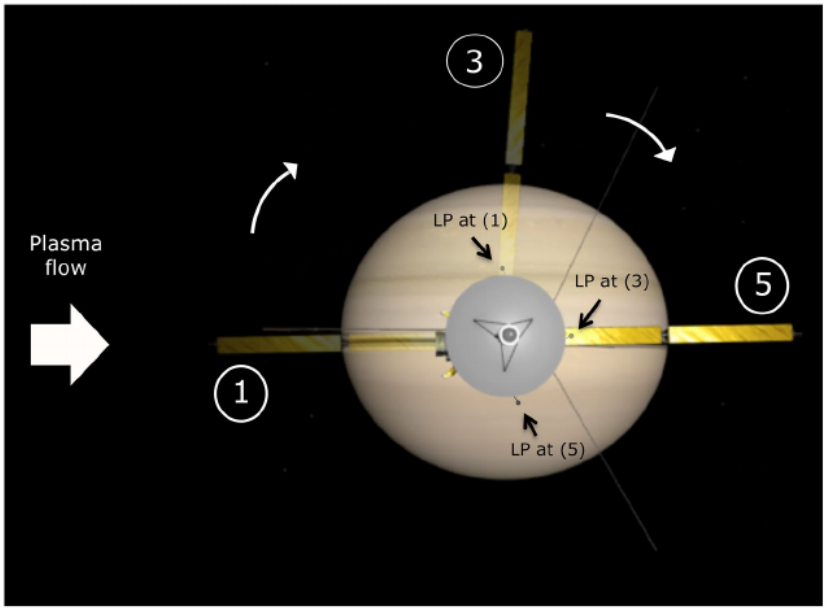

Figure 3. Illustration of the spacecraft roll. Cassini is seen from above the HGA and with Saturn in the background. The plasma, coming from the left, is moving faster than the spacecraft, which is also moving to the right of the figure. The plasma will overtake the spacecraft and form an ion wake structure on the right side of the spacecraft. The ion wake structure is illustrated in Figures 4 and 5. In the beginning of the spacecraft roll, at (1), the LP is measuring the undisturbed ions, at position (3) the LP is in the ion wake, and at (5) the LP has again moved out into the undisturbed ion flow. The measured ion density during the roll is presented in Figure 7.

Table 1a
Environmental Parameters for Cassini's Trajectory on 2010-03-03 From 10:29 to 10:50, for the Radial Distances and Times 4.50 (10:29), 4.54 (10:33), 4.60 (10:39), 4.62 (10:43), and 4.70 (10:50) R_S

Parameter	Value	Reference
n_e	54.99, 49.99, 46.99, 45.99, 43.99 cm^{-3}	LP measurements, see Figure 7 blue line, assuming $n_i \approx n_e + n_{e,h}$
T_e	1.7, 1.8, 1.8, 1.9, 2 eV	Schippers et al. (2013), (in agreement with Livi et al. [2014], LP measurements)
$n_{e,h}$	0.01 cm^{-3}	Schippers et al. (2008)
$T_{e,h}$	300 eV	Schippers et al. (2008)
n_i	55, 50, 47, 46, 44 cm^{-3}	LP measurements before and after the ion wake encounter, see Figure 7 (in agreement with CAPS/IMS measurements, Holmberg et al. [2012], [2017])
$v_{i,\vartheta}$	27, 29, 31, 33, 35 km/s	LP measurements before and after the ion wake encounter, (in agreement with CAPS/IMS measurements, Wilson et al. [2009]; Holmberg et al. [2012]; Livi et al. [2014])
Ion species	H_2O^+	Young et al. (2005); Sittler et al. (2008); Felici et al. (2018)
v_{xSSQ} v_{ySSQ} v_{zSSQ}	8.67, 8.54, 8.36, 8.24, 8.04 km/s 13.25, 13.25, 13.24, 13.23, 13.22 km/s 0.05, 0.05, 0.05, 0.05, 0.05 km/s	Cassini ephemeris tool
$\|B\|$	240, 230, 220, 220, 210 nT	Estimated, assuming dipole field

Table 1b
The Ion Temperature T_i

T_i	8, 20, 70 eV	Sittler et al. (2006); Wahlund et al. (2009); Livi et al. (2014)

Note. Since the density and temperature of the hot electrons do not vary significantly over the studied radial range, the values $n_{e,h} = 0.01$ cm^{-3} and $T_{e,h} = 300$ eV have been used for all the Case 1 simulations. This also applies to the dominant ion species H_2O^+. The ion temperature T_i is not well constrained in the studied region, so three different temperatures listed in Table 1b, have been used for each of the five studied times, listed in Table 1a.

Abbreviations: LP, Langmuir probe; SSQ, Saturn Solar Equatorial.

The environmental parameters for Case 1 are presented in Table 1a and 1b. Column 1 gives the environment parameters, column 2 specifies the input values used in the simulations, and column 3 gives the references that the values were obtained from. Column 2 in Table 1a gives the environmental parameters for the five simulations listed in the same order as above.

Space plasmas are commonly well described by two Maxwellian or kappa distributions for the electron population and one Maxwellian distribution for the ions. We have assumed two Maxwellian distributions for the electrons, describing a cold population with density n_e and temperature T_e and a hot population with density $n_{e,h}$ and temperature $T_{e,h}$. The validity of this assumption is further discussed in Section 3.3. The plasma is assumed to be quasineutral, i.e., the ion density $n_i \approx n_e + n_{e,h}$.

The used plasma densities are estimated from the RPWS/LP measurements recorded before and after the wake encounter. The density range from 44 to 55 cm^{-3} (excluding the wake measurements) for the time period covering the wake encounter. The used ion density values are listed in Table 1a and presented in Figure 7 (blue dots) where the simulated densities are compared to the measured ion densities. Usually the LP ion density measurements can be compared to both CAPS ion density measurements and RPWS electric field antenna electron density measurements. However, there is no good quality data available from CAPS for the ion wake encounter due to the roll of the spacecraft, but there are measurements available for the time interval just after the wake encounter. The CAPS/IMS ion density measured from 10:53 to 11:07 range from 45–49 cm^{-3} (LANL) and 46–50 cm^{-3} (LASP), which agrees very well with ion densities measured by the LP, see Table 1a. The cold plasma density is also in good agreement with the electron density estimated from the RPWS electric field antennas, which is measured to vary between 56 and 68 cm^{-3} during the time range from 10:29 to 10:50. Note that the ion wake is not detected in the RPWS electric field antenna measurements since the antennas are 10 m long and extend well beyond the impact of the ion wake. In addition, the RPWS electric field antenna measurements provide electron densities and not ion densities.

Schippers et al. (2013) used around 8 years of RPWS high-frequency power spectrum measurements to obtain the cold electron temperature and density in the region 2.8 to 10 R_S. They showed that the cold electron temperature within 4.8 R_S is well described by the power law $T_c\,(R < 4.8R_S) \approx 0.03\ R^{2.7\,\pm\,0.1}$ eV, which was used to obtain the cold electron temperature listed in Table 1a. Outside of 4.8 R_S the cold electron temperature decreases with increasing distance and is well described by $T_c\ (4.8 < R < 9R_S) \approx 3.3\ R^{-0.3\,\pm\,0.1}$ eV, which was used for the cold electron temperature listed in Table 2a. Schippers et al. (2008) illustrated the bimodal distribution functions that should be used to accurately represent the electron population present in the inner and middle magnetosphere of Saturn. They showed that the electron energy distribution is well represented with two Maxwellian or kappa distributions, one for the cold (<100 eV) population and one for the hot (100 eV–10 keV) population. Schippers et al. (2008) showed that in the region 4.5–5 R_S the density of the hot electron population is commonly around 0.01 cm^{-3} and with a temperature of 300 eV. Due to the low density of the hot electron population it will not have a significant contribution to the charging of the spacecraft, neither through electron accumulation nor through the production of secondary electrons.

It is a well known phenomena that plasma in the inner part of magnetospheres rotates with the planet, often with a speed close to the rotation frequency of the planet. This is also the case for Saturn's inner and middle magnetosphere, but the corotation enforcement currents are not strong enough to bring the plasma up to full corotation outside of three R_S (Pontius & Hill, 2009; Wilson et al., 2009; Holmberg et al., 2012). We obtain the subcorotation speed, that is, the azimuthal ion velocity $v_{i,\theta}$, from the RPWS/LP and CAPS measurements. The LP cannot provide flow velocities during the ion wake encounter since the spacecraft is blocking the plasma flow, but the azimuthal ion velocity $v_{i,\theta}$ just before and after the event range from 26 to 36 km/s, with an average of 30 km/s. This agrees very well with the fit to the $v_{i,\theta}$ measured by the RPWS/LP over 5 years and presented by Holmberg et al. (2012). They stated that $v_{i,\theta} = 1.5r^2 - 8.7r + 39$, in the region 3.1 to 6.7 R_S, which gives $v_{i,\theta}(4.5\ R_S) \approx 30$ km/s and $v_{i,\theta}(4.7\ R_S) \approx 31$ km/s. This is also in agreement with the CAPS measurements of $v_{i,\theta}$ just after the ion wake encounter, which shows 36–38 km/s (LANL) and 34–36 km/s (LASP). It is also consistent with CAPS measurements presented by Wilson et al. (2009) who showed $v_{i,\theta}(4.5\ R_S) = 35$ km/s and $v_{i,\theta}(4.75\ R_S) = 38$ km/s. In addition, the estimated velocities are confirmed by the average flow velocities presented by Livi et al. (2014), who showed $v_{i,\theta}(4.5\ R_S) \approx 28$ km/s and $v_{i,\theta}(4.7\ R_S) \approx 33$ km/s, estimated from around 6.5 years of CAPS measurements.

The plasma environment in the studied region consists mainly of water group ions W^+ (O^+, OH^+, H_2O^+, H_3O^+), hydrogen ions H^+, and electrons, with the water group ions (mainly H_2O^+) being the dominant ion species, see e.g., Young et al. (2005), Sittler et al. (2008), Wilson et al. (2015) and Felici et al. (2018). For simplicity, we have used H_2O^+ ions as the simulated ion species since minor variations in the ion mass has an insignificant impact on the final results.

The velocity of Cassini is given by the Cassini ephemeris tool, which is publicly available and provided by the RPWS group at University of Iowa. The spacecraft velocities stated in Table 1a are given in the SSQ coordinate system, defined in Section 2.1.

No magnetic field measurements are available for the studied time interval. Instead we estimate the magnetic field strength, assuming that the magnetic field of Saturn is dipolar, in the equatorial plane at radial distance $4.5 < r < 4.7\ R_S$ to $207 < |B| < 236$ nT using $B = B_0(R_S/r)^3$, where $B_0 = 21.5\ \mu$T is the estimated equatorial field strength of Saturn. The assumption of a dipolar field is valid within 6 R_S, beyond this distance the ring current adds a small perturbation field (Arridge et al., 2009). The assumption is also confirmed by MAG measurements in the same region at other time intervals, for example from 2010-02-13 21:25 to 21:35 when MAG measured $|B| = 195$–208 nT. The impact of the used magnetic field estimate on the final simulation results is further discussed in Section 3.3.

The position of the spacecraft in SSQ coordinates is given in the Supporting Material, which also gives the transformation from SSQ to the spacecraft coordinate system for the plasma flow, spacecraft velocity, and magnetic field. The transformed parameters, listed in Table S3, are used for the simulations.

Most studies presenting estimates of the ion temperatures in the inner and middle part of Saturn's magnetosphere are based on Cassini/CAPS measurements. However, the CAPS measurements within 5.5 R_S should be used with great care since it is known that a significant amount of penetrating background radiation contaminates the measurements within this distance, see e.g., Young et al. (2004), Elrod et al. (2012), and

Livi et al. (2014). Another perturbation, for the LASP CAPS data, is the large amount of pick-up ions within 5.5 R_S. The LASP fit assumes Maxwellian distributions and does not include the impact of the pickup-ions (Wilson et al., 2017). Reliable water group ion temperatures T_{W+} and hydrogen ion temperatures T_{H+} are therefore not available for the studied time interval. Instead we use a combination of CAPS and RPWS/LP measurements and our simulation results to obtain a likely range of the ion temperature in the studied region. The ion temperature measured on June 30, 2004 for the region within 6 R_S is presented in Sittler et al. (2006). They estimate a T_{W+} of around 35 eV and a T_{H+} of around 3 eV at 4.5–4.7 R_S. Livi et al. (2014) used around 6.5 years of CAPS data for a statistical study of the plasma parameters. They presented $T_{W+} \approx 70 \pm 60$ eV, which shows the uncertainty of the temperature estimates in this region. The CAPS/IMS T_{W+} measured from 10:53 to 11:07 range from 39–42 eV (LANL) and 44–48 eV (LASP). Wahlund et al. (2009) used measurements from two Cassini orbits in 2005 and 2006 to estimate an upper limit for the T_{W+} in the region around 4–5 R_S. They obtained $T_{W+,max} \approx 8$ eV. Considering this wide range of presented ion temperatures we have used three different temperatures for the simulations in order to estimate the impact of varying T_{W+}. The temperatures used are $T_{W+} = 8$ eV based on the results by Wahlund et al. (2009), $T_{W+} = 20$ eV, and $T_{W+} = 70$ eV based on the results by Livi et al. (2014). For each of the five studied time intervals three simulations with the different ion temperatures have been performed, bringing the total number of simulations for Case 1 to 15. The temperature $T_{W+} = 20$ eV and the plasma densities listed in Table 1a gives a Debye length between 1.2 and 1.4 m.

2.4. The Environment of Case 2

We have also simulated the ion wake structure at around 7.6 R_S in order to illustrate the difference between the ion wake structures formed in the inner and middle magnetosphere of Saturn. Two clear ion wake signatures were detected at 2005-12-24 during the time intervals 11:08-11:16 and 11:36-11:43. For a rough comparison with the measured wake densities, we only simulate the spacecraft - plasma interaction in the environment at 11:13, that is when the LP is in the center of the ion wake and the measured ion density is at a minimum. The environment parameters used for the simulations are listed in Table 2a and 2b, and the measured ion density is presented in Figure 8 (blue dots) where the simulated densities are compared to the measured ion densities. The CAPS/IMS density at 11:13 is estimated to 14 cm^{-3} (LASP), which is in agreement with the ion density estimated from the LP measurements performed before and after the ion wake encounter. The azimuthal ion velocity measured by CAPS/IMS is estimated to 61 km/s (LASP), which also is in good agreement with the LP measurements. It is in good agreement with both the LP measurements recorded before and after the ion wake encounter and the velocity obtained from the statistical study presented in Holmberg et al. (2012). The parameters listed in Table 2a are all obtained from the references discussed in Section 2.3, except for the magnetic field strength $|B|$. MAG measurements are available during the time interval of Case 2 and the measured $|B|$ is presented in the last row of Table 2a.

The CAPS ion temperature measurements recorded at 7.6 R_S from Saturn are not perturbed to the same extent as at 4.5 R_S and are therefore more accurate. The CAPS ion temperature data still show a wide range for the studied time interval, ranging from 110 to 300 eV with 196 eV (LANL) and 157 eV (LASP) measured around the time 11:13. Sittler et al. (2006) presented $80 < T_{W+} < 120$ eV at around 7.6 R_S. Thomsen et al. (2010) presented equatorial $T_{W+} \approx 80$ eV, based on a statistical study of CAPS measurements from the first 4.5 years of the Cassini mission. To accommodate the wide range of estimated ion temperatures three simulations are performed, with $T_{W+} = 100$, 200, and 300 eV. The temperature $T_{W+} = 200$ eV and the plasma density listed in Table 2a gives a Debye length of around 2 m.

3. Results and Discussion

3.1. Case 1: The Ion Wake Structure

The SPIS simulations provide a global image of the ion wake structure. Figure 4 shows a cross-section of the simulated n_i in the yz-plane for the time 2010-03-03 at 10:29, so just before the LP enters the wake. The

Table 2a
Environmental Parameters for the Cassini Trajectory on 2005-12-24 at 11:13 and 7.6 R_S

Parameter	Value	Reference
n_e	24.85 cm^{-3}	LP measurements excluding the wake encounter, see Figure 8, assuming $n_i \approx n_e + n_{e,h}$
T_e	1.8 eV	Schippers et al. (2013) (in agreement with Livi et al. [2014])
$n_{e,h}$	0.15 cm^{-3}	Schippers et al. (2008)
$T_{e,h}$	1,800 eV	Schippers et al. (2008)
n_i	25 cm^{-3}	LP measurements excluding the wake encounter, see Figure 8, (in agreement with CAPS/IMS measurements Holmberg et al. [2012], [2017])
$v_{i,\theta}$	60 km/s	LP measurements excluding the wake encounter, (in agreement with CAPS/IMS measurements, Wilson et al. [2009], [2017]; Holmberg et al. [2012]; Livi et al. [2014])
Ion species	H_2O^+	Young et al. (2005); Sittler et al. (2008); Felici et al. (2018)
v_{xSSQ} v_{ySSQ} v_{zSSQ}	−8.52 km/s 8.42 km/s 0.08 km/s	Cassini ephemeris tool
$\|B\|$	35 nT	MAG measurements

Table 2b
The Ion Temperature T_i

T_i	100, 200, 300 eV	CAPS measurements, (in agreement with Sittler et al. [2006]; Thomsen et al. [2010]; Livi et al. [2014]; Wilson et al. [2017])

Note. The Ion Temperature T_i is not well constrained in the studied region, so three different temperatures have been used to simulate the spacecraft plasma interaction for Case 2.

Abbreviations: LP, Langmuir probe; SSQ, Saturn Solar Equatorial.

LP is not included in Figure 4 since it is located at $x = -2.288$ and the figure shows the yz-plane at $x = 0$. A depletion of ions, the ion wake, is formed behind the spacecraft with densities reaching down to around 10 cm^{-3}. The isolines marks 10, 20, 30, 40, and 50 cm^{-3}. The figure shows a cross section of the most depleted part of the wake.

Figure 5a shows the n_i in the xy-plane at $z = -0.489$, so at the height of the center of the LP, of the spacecraft for the date and time 2010-03-03 10:29. For Figures 4 and 5a the Sun is in the -z direction, Saturn is in z, the plasma flow in -y (thick white arrow) and the spacecraft velocity in the -yz direction (thin white arrow).

Figure 5 clearly shows the evolution of the ion wake, in the xy-plane, as the spacecraft is rolling. The different panels corresponds to the different times that are separated by an approximately 45° turn of the spacecraft in the xy-plane, panel (a) represents the configuration at 10:29, (b) at 10:33, (c) at 10:39, and (d) at 10:43. The roll of the spacecraft is also illustrated in Figure 3. The location of the LP is marked with a white star. The black line shows the lower part of the MAG boom. As can be seen in Figure 1 the LP is in the same plane in z as the gap that is located between the UEM (the upper part of the main spacecraft body) and the HGA. Since the plane at $z = -0.489$ does not contain any part of the main spacecraft body, we have included a black circle with the same size as the top of the UEM in all panels of Figure 5 to outline the size of the spacecraft just below this plane.

Figure 5 shows that the ion depletion extends more than 3 m from the spacecraft. As Cassini is moving from 4.5 (at 10:29) to 4.62 R_S (at 10:43) it is moving away from the main plasma source Enceladus, hence the plasma density is decreasing. The plasma density used for the simulations is decreasing from 55 to 46 cm^{-3}, the decrease in plasma density and the simultaneous increase in the plasma flow velocity is impacting the ion density in the wake. The wake created at 4.62 R_S (10:43), Figure 5d, has a larger region with ion densities even below 10 cm^{-3}, reaching down to just 2 cm^{-3}. Figure 5 shows that, without detailed simulations, it can be difficult to predict if a certain instrument, such as the Langmuir probe or CAPS, will be located within the wake region for a certain environment and spacecraft orientation. For example, the wake structure

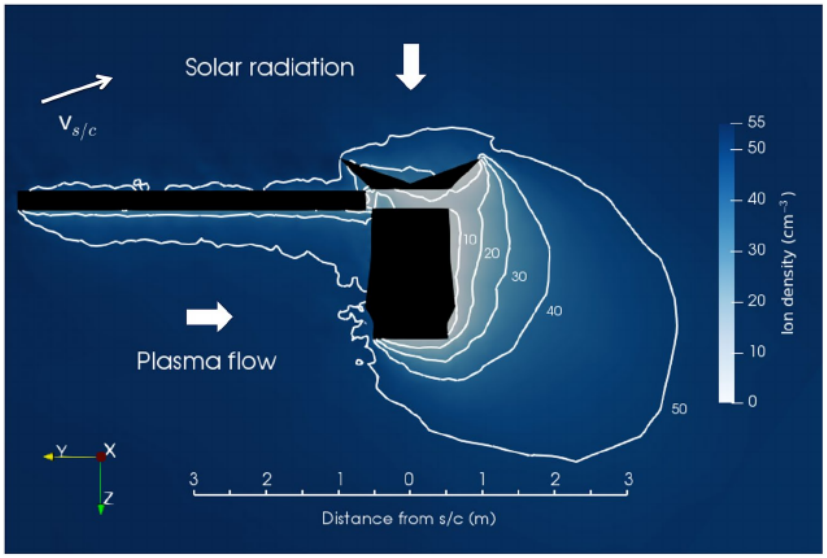

Figure 4. Cross-section of the ion density around Cassini, in the yz-plane at $x = 0$, for the time 2010-03-03 10:29. The Sun is in the -z direction, the plasma flow of 27 km/s is in the -y direction, and the spacecraft is moving with $v_{s/c,x} = 0$ km/s, $v_{s/c,y} = -13.3$ km/s, and $v_{s/c,z} = -8.7$ km/s. The depletion of ions due to the presence of the spacecraft extends more than 3 m away from the spacecraft.

shown in Figure 5b shows a depletion of ions also in front of the spacecraft. This is due to the z component of the spacecraft velocity that is causing the HGA to block the plasma flow from above, which creates a small depletion in front of the spacecraft.

3.2. Case 1: Additional Simulation Results

Figure 6 shows additional simulation results, such as (a) the electron density, (b) the photoelectron density, (c) the secondary electron density and (d) the potential structure around the spacecraft, in the plane that contains the z axis and the center of the LP. Figure 6 show the parameters obtained when simulating the environment at the time 2010-03-03 10:29, the same time as for Figures 4 and 5a. For this environment Cassini charged down to −5.1 V. The potential structure around the spacecraft is shown in Figure 6d. A negative potential was obtained since the electron density of the studied environment is large enough to result in a higher accumulation of electrons on the surface than the accumulation of ions and the emission of secondary electrons and photoelectrons. The spacecraft surface potential of −5.1 V agrees very well with the estimates presented by Livi et al. (2014), which range from −2 V to −8 V with average values from −5 to −5.5 V for the region between 4.5 and 4.7 R_S. The simulation also provide a floating potential U_{float}, which is the potential measured at the location of the LP, of around −2.2 V, which is in good agreement with the potential of between −2 and −3 V measured by the LP. Figure 6a shows that the negative surface potential will repel the ambient electrons and prevent them from reaching the surface of the spacecraft, resulting in the electron density reaching down to just a few cm^{-3} closest to the spacecraft.

The LP cannot separate between photoelectrons and secondary electrons originating from the spacecraft and electrons of magnetospheric origin, but it is clear from Figure 6c that the secondary electrons from the spacecraft, with a maximum density of around 0.25 cm^{-3} and a density of 0.07 cm^{-3} at the location of the LP, will not have a significant effect on the electron measurements for this particular environment. This is also true for the photoelectrons, see Figure 6b, with a maximum density of around 3 cm^{-3} in the center of the HGA and a density close to 0 cm^{-3} at the location of the LP. Hence, the impact on the LP measurements of secondary electrons and photoelectrons originating from the spacecraft is negligible, for the studied environment. However, there is also a contribution of secondary electrons and photoelectrons originating from the probe itself, which will most likely affect the LP measurements (Wang et al., 2015). In order to study this effect, detailed SPIS simulations of the LP and its measurements are needed. Since our study is focused on

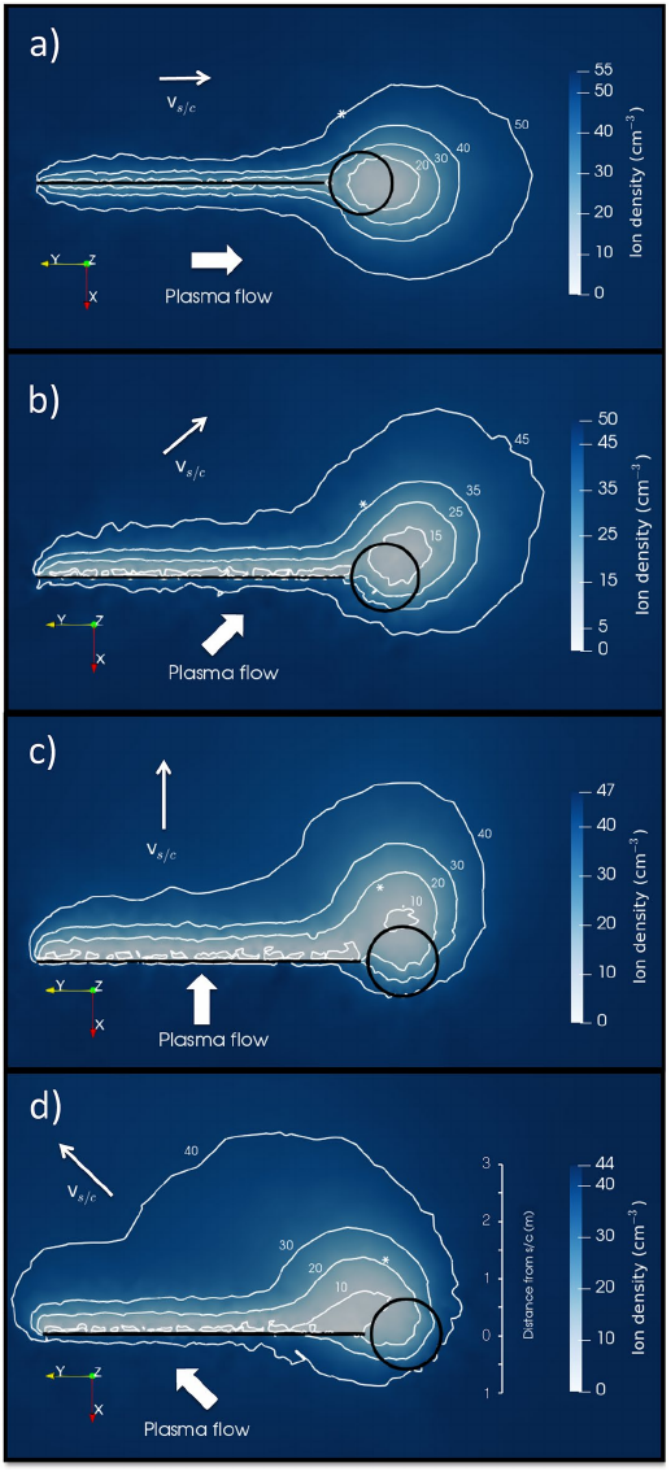

Figure 5. Cross-sections of the ion density around Cassini, in the xy-plane at $z = -0.489$, for four different time intervals during 2010-03-03. The figure shows the evolution of the ion wake as the spacecraft is rolling. Panel (a) represents the configuration at 10:29, (b) at 10:33, (c) at 10:39, and (d) at 10:43. The black circle outlines the spacecraft body and the position of the LP is marked with the white star. Please note that the ambient plasma density is decreasing as Cassini is moving outwards in Saturn's magnetosphere, so the color scale is different from panel (a) through (d).

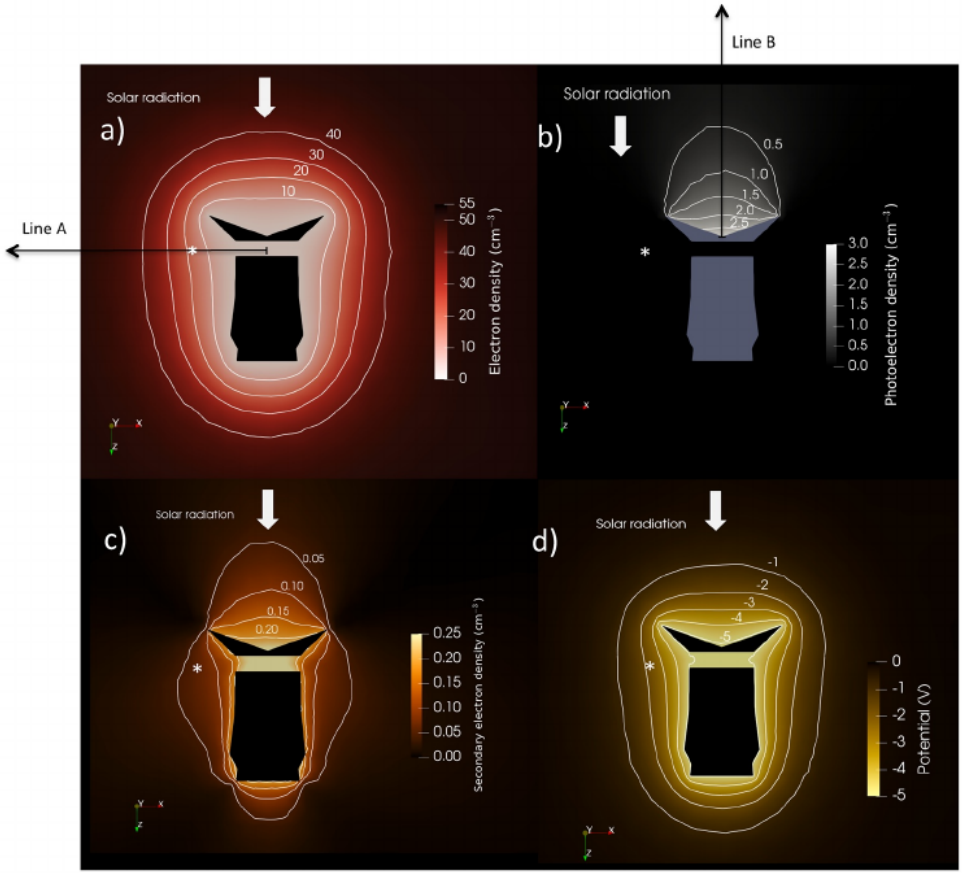

Figure 6. Cross-section of (a) the electron density n_e, (b) the photoelectron density n_{ph}, (c) the secondary electron density n_{se}, and (d) the potential, for the time 2010-03-03 10:29 and in the plane that contains the z axis and the center of the Langmuir probe (LP). The white marker shows the position of the LP. The white arrow shows the direction of the solar radiation. (a) The n_i, n_e, n_{se}, and the potential shown in Figure 9 are all given along Line A. (b) n_{ph} in Figures 9a and 9b is given along Line B.

the impact of the spacecraft body on the LP measurements, detailed simulations of the LP measurements is beyond the scope of this article and therefore left for future work.

Figure 6a also shows Line A, which is the line the parameters n_i, n_e, n_{se}, and the potential presented in Figure 9 are all given along. The parameters n_{ph} presented in Figures 9a and 9b are given along Line B, which is shown in Figure 6b.

Figures 4–6 demonstrate what happens to a spacecraft located in a dense and cold plasma. An ion wake will form if the relative speed of the spacecraft exceeds the ion thermal speed, this is shown in Figures 4 and 5. Commonly the frequency of electrons hitting the spacecraft is larger than that of the ions, due to the electrons larger thermal velocity, which will charge the spacecraft negatively (see Figure 6d). The negative spacecraft potential will repel electrons (see Figure 6a). Photoelectrons will be emitted from the sunlit parts of the spacecraft (see Figure 6b) and the impacting electrons and ions will knock out electrons from the spacecraft (see Figure 6c). The final spacecraft potential is given by the balance of all these currents to and from the spacecraft. The current balance for Cassini, for the environment presented in Figures 4, 5a, and 6, is given by

$$I_{e,c} \approx I_i + I_{ph,e} + I_{se,e} \tag{1}$$

where $I_{e,c}$ is the cold electron current, I_i the ion current, $I_{\mathrm{ph},e}$ the emitted photoelectron current, and $I_{\mathrm{se},e}$ is the emitted secondary electron current. The collected photoelectron current $I_{\mathrm{ph},c}$, the collected secondary electron current $I_{\mathrm{se},c}$, and the hot electron current $I_{e,h}$ are all negligible. This is because the negative potential

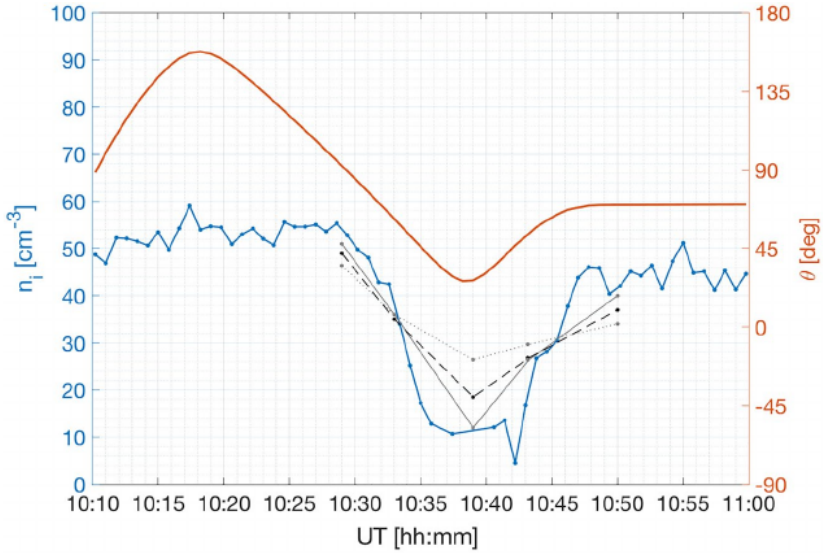

Figure 7. The measured ion density n_i (blue) and the angle θ (red) between the corotation direction and the Langmuir probe (LP) for the time interval 2010-03-03 10:10 to 11:00. The simulated density at the position of the LP is given by the gray dots. The simulated densities are obtained when using $T_i = 8$ eV (connected with solid gray line), 20 eV (dashed gray line), and 70 eV (dotted gray line).

of the spacecraft will repel the vast majority of the produced secondary electrons and photoelectrons, which both have a temperature of 2 eV. The contribution from the hot electrons is negligible because of the low hot electron density compared to the cold electron density.

3.3. Case 1: Comparision With Cassini LP Measurements

Figure 7 shows the measured (blue dots) and simulated (gray and black dots) ion density in the ion wake behind Cassini. Figure 7 also shows the angle θ between the corotation direction, that is, the direction of the plasma flow, and the Langmuir probe (red line). The figure shows how the measured ambient plasma density decreases as the Langmuir probe moves into the ion wake at around 10:30 and $\theta \approx 70°$ and increases again as the LP move out of the ion wake at around 10:40. At around 10:46 and $\theta \approx 65°$ the Langmuir probe has left the wake region and is again measuring the undisturbed plasma. Please note that θ is not limited to the plane orthogonal to the plasma flow plane, which is why θ does not reach down to 0 even though the LP crosses the plane of the plasma flow at 10:39. The simulated ion density, presented in Figure 7, is the one obtained at the location of the LP for the three different ion temperatures, $T_i = 8$, 20, and 70 eV and for the five different environments and spacecraft orientations presented in Section 2.3 and Table 1a. Each density value has been estimated from a mean of the simulated ion densities found in a sphere with radius 5 cm and centered at the center of the LP location. The mean values of the simulated densities obtained when using $T_i = 8$ eV (light gray dots), 20 eV (black dots), and 70 eV (gray dots) are connected with a light gray solid line, dashed black line, and dotted gray line, respectively. The best agreement with the measured ion density (blue dots) is obtained with $T_i = 8$ eV. Figure 7 also shows that the difference in the simulated ion density outside of the wake is negligible for the three different ion temperatures. The ion temperature dependence is strongest in the innermost part of the wake. The disagreement between the measured ion density in the Cassini spacecraft wake and the simulated densities using $T_{W+} > 20$ eV, indicates that the ion temperature estimates based on CAPS measurements, for example $T_{W+} = 70 \pm 60$ eV by Livi et al. (2014), $39 < T_{W+} < 42$ eV by CAPS/IMS (LANL) and $44 < T_{W+} < 48$ eV by CASP/IMS (LASP), are overestimated. The results presented in Figure 7 suggest that the water group ion temperature in the region 4–5 R_S is closer to the range 5–15 eV.

Considering the simulated ion densities in the regions that are not strongly temperature dependent, meaning outside of the innermost part of the ion wake, the good agreement between the simulated densities

and the measured ion densities shows that our assumptions, stated in Section 2.3, are valid and provide accurate simulation results. For example, using a Maxwellian instead of kappa distribution for the cold electrons will produce a slightly lower density estimate of electrons intermediate between the cold and the hot component (see Schippers et al., 2008, their Figure 2). Slightly higher densities for electrons in this energy range, ~100 eV, could result in a larger amount of produced secondary electrons and less negative spacecraft surface potential. However, as indicated by the good agreement between the measured and simulated ion density outside of the wake, presented in Figure 7, the impact on the final simulation results would be insignificant.

Using a Maxwellian instead of kappa distribution for the hot electron population will also result in an underestimation of the hot electrons with energies above ~20 keV (see Schippers et al., 2008, their Figure 2). However, this will not impact the simulation results since the contribution of the hot electron population to the spacecraft - plasma interaction is small or negligible in the studied regions. For Case 1, this is shown in the current balance in Equation 1. This was also confirmed by running two simulations using kappa distributions for the hot electron component. The used simulation set-ups was the ones for Case 1 at time 10:39 with $T_i = 8$ eV and for Case 2 with $T_i = 200$ eV. The resulting density difference, between the simulations using a Maxwellian or a kappa distribution, was less than 0.1 cm^{-3}.

A test simulation also showed that the magnetic field strengths in the studied regions are too weak to impact the spacecraft - plasma interaction. A simulation using a magnetic field strength twice the value listed in Table 1a, for Case 1 at 10:39 with $T_i = 8$ eV, generated no changes in the simulated potential and ion density values.

In addition, one simulation with a more detailed spacecraft model (not shown) was performed in order to investigate if the used spacecraft model, depicted in Figure 1c, was too simplified. In order to study if parts of the spacecraft located in between the HGA and the UEM, that were not included in the simulations, could obstruct the plasma flow and result in lower simulated ion densities than the ones presented. However, simulations including obstructive objects, such as the Radio Frequency Electronics Subsystem (RFES), between the HGA and the UEM resulted in insignificant differences in the simulated ion densities, lower than 0.5 cm^{-3}. This indicated that the chosen simplified spacecraft model fulfilled the criteria of saving simulation time without losing accuracy in the simulated parameters.

3.4. Case 2: Simulation Results

As was stated in Section 2.2, we also performed simulations for the ion wake formation at 7.6 R_S from Saturn, referred to as Case 2. Figure 8 shows the measured RPWS/LP ion density (blue dots) for the date 2005-12-24 and time interval 10:55 to 11:55. Figure 8 also shows the angle θ between the corotation direction and the Langmuir probe (red line). The figure shows that the Langmuir probe is measuring lower plasma densities when located in the ion wake during the time intervals around 11:08-11:16 and 11:36-11:43. The simulated ion density in the innermost part of the wake, at 11:13, is also shown in Figure 8. Three different ion temperatures were used, $T_i = 100$ eV (orange dot), 200 eV (black), and 300 eV (light gray). The different temperatures gives a density of 9, 12, and 13.5 cm^{-3} respectively. The simulated densities, using an ion temperature of both 200 and 300 eV, are in very good agreement with the measured density of around 13 cm^{-3}, as can bee seen in Figure 8. In this region, the ion wake structure is not as prominent as it is in the denser plasma at 4.5 R_S. This is due to the lower plasma density and the higher ion temperature at 7.6 R_S. For this environment Cassini charged to −3.4 V, shown in Figure 9c, which is in good agreement with the statistical estimates of Livi et al. (2014), which range from −0.7 to −5 V with an average of −3 V at 7.6 R_S. The simulated floating potential is −2.0 V, which is in good agreement with the measured floating potential of −2.2 V.

Since the ambient plasma density is lower and the hot electron density is higher at 7.6 R_S than at 4.5 R_S, the hot electron component has a more important role, both by increased accumulation of hot electrons but also by producing more secondary electrons. The current balance at 7.6 R_S is given by

$$I_{e,c} + I_{e,h} \approx I_i + I_{ph,e} + I_{se,e} \quad (2)$$

where $I_{e,h}$ is the hot electron current. The $I_{se,c}$ and $I_{ph,c}$ are negligible due to the negative surface potential obtained in this environment. More secondary electrons are produced in Case 2 than in Case 1, resulting

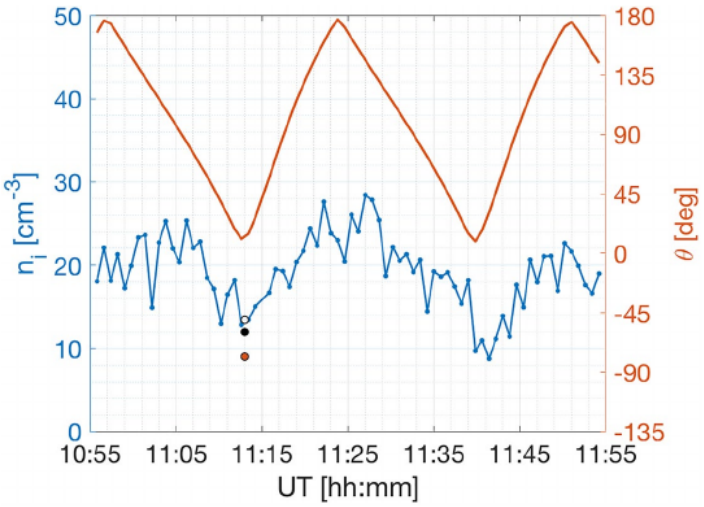

Figure 8. The measured ion density n_i (blue) and the angle θ (red) between the corotation direction and the LP for the time interval 2005-12-24 10:55 to 11:55. Two wake structures can be seen around the time intervals 11:08-11:17 and 11:36-11:43. However, the detected wake structures are not as clear and the depletions are not as large as what can be detected around 4.5 R_S shown in Figure 7. The figure also shows the simulated densities for the environment and spacecraft orientation at 11:13 using $T_i = 100$ eV (orange dot), $T_i = 200$ eV (black dot), and $T_i = 300$ eV (light gray dot). The different temperatures gives a density of 9, 12, and 13.5 cm^{-3}, respectively.

in a maximum secondary electron density of 4.3 cm^{-3} and a density of 0.8 cm^{-3} at the location of the LP. The simulated photoelectron density for Case 2 does not differ significantly from the photoelectron density of Case 1. The photoelectron density depends on the distance to the Sun, the spacecraft materials, and the spacecraft orientation. Since these parameters are very similar for the two cases, the change in the production of photoelectrons from the spacecraft is insignificant. Hence, the secondary electrons and photoelectrons originating from the spacecraft will not impact the LP measurements in this environment.

3.5. Comparision of Simulation Results From Case 1 and 2

Figure 9 shows a comparison between the simulated densities and potentials estimated in the most depleted part of the ion wake for the times 2010-03-03 10:39 (Case 1) and 2005-12-24 11:13 (Case 2). The potentials and densities, except for the photoelectron density, are given along a line of 8 m between the points (0, 0, −0.489) m and (−7.670, 2.222, −0.489) m. The line, referred to as Line A, is shown in Figure 6a and lays in the plane depicted in Figure 5. The line passes the location of the LP at (−2.288, 0.663, −0.489) m, which corresponds to the distance 2.43 m, marked with vertical black lines in Figure 9. Figures 9a and 9b show the simulated ion density n_i (dark gray solid line), electron density n_e (black dashed line), secondary electron density n_{se} (black dash-dotted line), and photoelectron density n_{ph} (light gray solid line). Figure 9c shows the potentials along Line A for the time 2010-03-03 10:39 (dark yellow dashed line) and 2005-12-24 11:13 (yellow solid line). The HGA is shielding the spacecraft body from the Sun, see Figure 6b, resulting in a negligible amount of photoelectrons emitted from the sides of the spacecraft. The n_{ph} in Figures 9a and 9b are therefore not along the same line as the n_i, n_e, and n_{se}. The n_{ph} is instead given along a line from the middle of the HGA at (0, 0, −1.149) m to (0, 0, −9.149) m, shown as Line B in Figure 6b.

Figure 9a shows the simulated n_i, n_e, n_{se}, and n_{ph} for the time 2010-03-03 10:39. The first ∼1 m shows the particle densities within the gap between the Cassini spacecraft body and the HGA. The ions are obstructed by the spacecraft body and the HGA but part of the flow is able to pass through the gap between the spacecraft and the HGA, this explains the decrease in ion density over the first ∼1 m. Figure 9a shows that the plasma is disturbed out to about 6 m from the center of Cassini where $n_i = n_e = 47$ cm^{-3}, which is the density of the ambient plasma. Both Figures 9a and 9b show $n_e < n_i$ within the sheet around the spacecraft. Cassini is charged a few volts negative for both environments, shown in Figure 9c. Since the electron temperature is only 1.7–2 eV, a large portion of the cold electron population will be repelled before reaching the spacecraft,

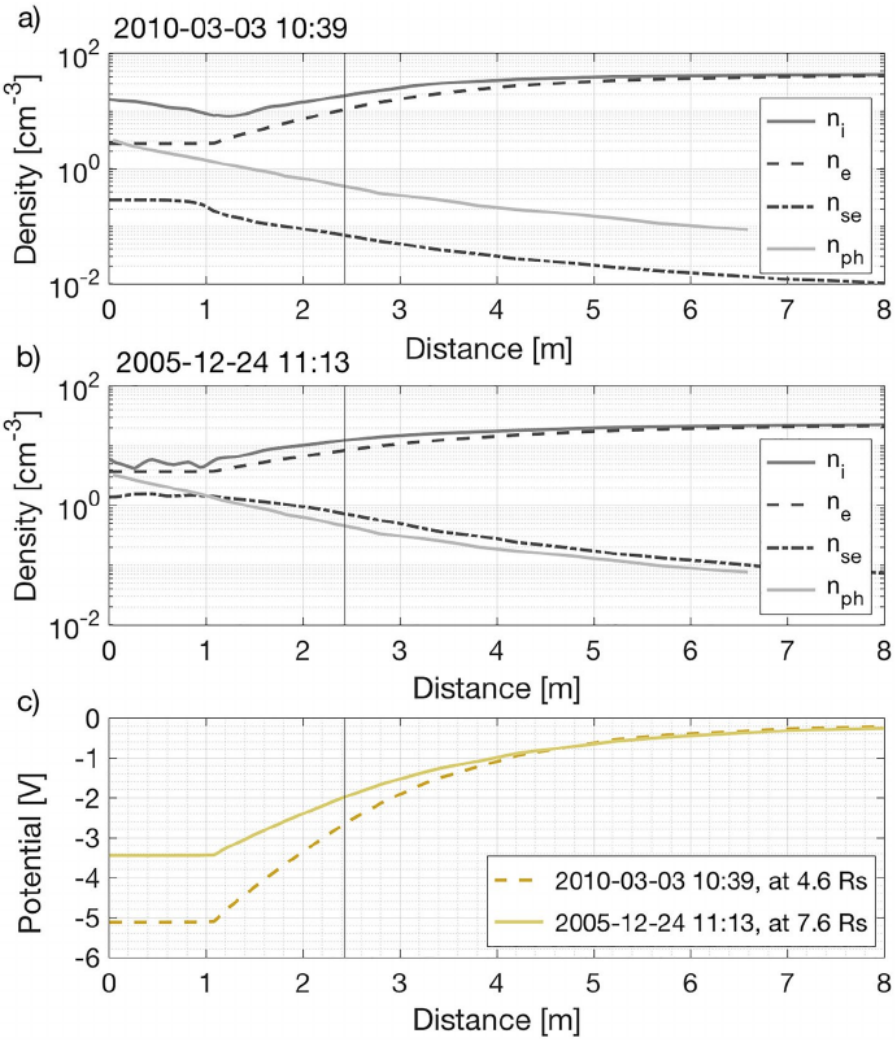

Figure 9. (a) The simulated ion density n_i (dark gray solid line), electron density n_e (black dashed line), secondary electron density n_{se} (black dash-dotted line), and photoelectron density n_{ph} (light gray line) in the most depleted part of the ion wake for the time 2010-03-03 10:39 (Case 1). The parameters n_i, n_e, and n_{se} are given along an 8 m distance, shown as Line A in Figure 6a, which passes the location of the LP at 2.43 m (vertical black lines). The photoelectron density n_{ph} (light gray line) is instead given along Line B, shown in Figure 6b, since the orientation of the spacecraft is resulting in a negligible amount of photoelectrons being produced along Line A. (b) Same set up as in (a) but for the time 2005-12-24 11:13 (Case 2). (c) The simulated potentials along Line A at 2010-03-03 10:39 (dark yellow dashed line) and 2005-12-24 11:13 (yellow solid line).

which is illustrated in Figures 9a (black dashed line), 9b (black dashed line), and 6a. A larger depletion of electrons is detected at 4.6 R_S than at 7.6 R_S due to the higher plasma density and surface potential of the spacecraft.

The ion wake is also clearly visible as the depletion of ions in both Figures 9a and 9b. This depletion is not due to the charging of the spacecraft but to the obstruction of the ions in the plasma flow, and therefore only visible behind the spacecraft as shown in Figures 4 and 5. How depleted the wake is depends on the ion energy. Figure 7 shows how the prominence of the ion wake is reduced when the ion temperature is increasing. This suggests that if the ion temperature is high enough no wake would be detected. Figures 9a and 9b also shows the difference in n_{se} (black dash-dotted lines) between the two environments. As described earlier, the lower $n_{e,c}$ and higher $n_{e,h}$ will increase the production of secondary electrons at 7.6 R_S, Figure 9b, compared to at 4.5 R_S, Figure 9a. In addition, Figures 9a and 9b show that the difference in n_{ph} (light gray

solid line) between the two cases are negligible. This is due to the same part of the spacecraft being sunlit and the same solar radiation flux being used for both simulations. Figure 9c shows the simulated potentials for both Case 1, at 4.5 R_S, (dark yellow dashed line) and Case 2, at 7.6 R_S, (yellow solid line) along Line A. The values between 0 and 1 m give the surface potentials of the spacecraft. The higher plasma density at 4.5 R_S gives rise to a more rapid decrease in the potential from this environment (dark yellow dashed line) than of the potential at 7.6 R_S (yellow solid line). Figure 9c shows that the potential structure generated by Cassini extends to a distance of more than 8 m from the spacecraft, which is expected given the Debye length.

It is important to point out that the small amount of LP measurements of the Cassini ion wake early on in the mission is the reason why good statistics of the ion density and ion velocity could be produced without correcting for ion wake measurements, shown in Holmberg et al. (2012). This was not true later on in the mission when spacecraft calibration rolls started to be performed more often in the denser part of the plasma disk, thus producing more significant and a larger amounts of ion wake measurements, shown in Holmberg et al. (2017).

4. Conclusions

Accurate analyses of the Cassini data include a full understanding of any significant perturbations, in particularly disturbances from the spacecraft itself. In this study we show that the Cassini LP ion density measurements are significantly impacted by the presence of an ion wake, which is formed behind Cassini in certain environments. The study shows that the ambient plasma density can be more than five times larger than the measured ion wake density, see Figure 7. This shows the importance of detecting wake measurements and excluding them from estimates of the ambient plasma density, to prevent the ion wake density decrease from being mistaken for actual density decreases found in the Kronian system, such as for example interchange injection events or moon wakes.

The comparison between the simulated and the measured parameters (ion density, spacecraft potential, and floating potential) shows that SPIS can be used, with high accuracy, to simulate the spacecraft potential and the spacecraft plasma interaction in plasma regimes similar to the ones studied here. The studied plasma environment is a common environment for the inner and middle magnetosphere of Saturn, and it is not substantially different, in terms of the ability to induce spacecraft surface charging, from plasma environments found in the magnetospheres of Jupiter, Uranus, Neptune, and Earth, in the solar wind and in the induced magnetospheres of Mars and Venus. This is an important result, since SPIS simulations are commonly used to study the expected spacecraft surface potential in preparation for future missions. Despite this, SPIS simulation results have seldom been confirmed by actual in-situ measurements, as has been done in this study. The results from this study serve as a confirmation that SPIS simulations will produce a realistic and accurate result in typical magnetospheric conditions, when surface material properties and environment parameters are known and used correctly. This is particularly relevant for future interplanetary missions currently in development, such as JUICE and Europa Clipper, where SPIS simulations can be used for risk analyses, to prepare for future data analyses, and to optimize both spacecraft and instrument operations.

Our simulation results are also used to better constrain the ion temperature which is a parameter that is difficult to estimate in the inner magnetosphere of Saturn, within around 5.5 R_S, due to the penetrating background radiation that is known to contaminate the CAPS measurements and the impact from pick-up ions on the ion phase space distribution (e.g., Young et al., 2004; Elrod et al., 2012; Livi et al., 2014; Wilson et al., 2017). The simulation results indicate that the ion temperature around 4.5 R_S should be <20 eV in order to explain the large depletion of ions behind the spacecraft, see Figure 7. The ion temperature which gives the best fit, of the studied temperatures, is $T_i = 8$ eV, which is in accordance with the estimates of Wahlund et al. (2009). The results indicate that the estimate of Livi et al. (2014) of 70 ± 60 eV is overestimated. A correct estimate of the plasma parameters of Saturn's magnetosphere is important, not only to have an accurate understanding of the environment itself, but also to have accurate input for simulations and models of the system.

We also conclude that the disturbance in the plasma density measurements of the LP, due to the presence of the ion wake, can occasionally be seen already at around 70° angle between the corotation direction and

the LP. However, a vast majority of the detectable ion wake encounters are located within 4–6 R_S and in the later part of the Cassini mission and they have therefore only caused minor perturbations to the LP data analyses (Holmberg et al., 2017). Less than 15 wake signatures could be found at 7.6 R_S, with most of them consisting of only one data point.

The simulations show that the depletion of ions, that is the ion wake, will extend out to around 6 meter behind the spacecraft, with a larger depletion found in the denser plasma region at ∼4.5 R_S compared to at 7.6 R_S. At 4.6 R_S the ion density will decrease from the ambient plasma density of 47 cm^{-3} to 8 cm^{-3} in the center of the wake, shown in Figure 9a. At 7.6 R_S the ion density will decrease from the ambient plasma density of 25 cm^{-3} to 5 cm^{-3} in the center of the wake, shown in Figure 9b. The simulation results also provide the depletions of electrons around the spacecraft, shown in Figures 6a, 9a and 9b, due to the negative potential of the spacecraft, shown in Figures 6d and 9c. At 4.5 and 7.6 R_S the spacecraft will charge to −5.1 and −3.4 V, respectively. The simulated surface potentials are in very good agreement with average values of the spacecraft potentials obtained from the CAPS measurements (Livi et al., 2014) and the potentials measured by the LP.

We also conclude that the secondary electron and photoelectron populations originating from the spacecraft should be a minor disturbance to the LP measurements in the studied environments, due to the low density of both the secondary electrons and the photoelectrons compared to the ambient plasma density. The secondary electron and photoelectron populations originating from the LP is, however, of importance. In addition, for larger radial distances from Saturn or higher latitudes above the plasma sheet both the secondary electron current and the photoelectron current originating from the spacecraft should be of major importance. This can also be seen when comparing the density difference between the plasma density, n_e and n_i, in the sheet around the spacecraft and the secondary electron density n_{se} and the photoelectron density n_{ph} shown in Figures 9a and 9b. At 7.6 R_S, Figure 9b, the density difference has decreased compared to the difference at 4.5 R_S, Figure 9a. The difference will continue to decrease as the spacecraft moves further out in the magnetosphere, since the ambient plasma density will decrease and the hot electron density increase (leading to an increase in the secondary electron production), while the photoelectron production will stay the same for similar orientations of the spacecraft.

The surface potential of a spacecraft in space is described by a current balance, at equilibrium the sum of the currents is zero. For Cassini in the environments at 4.5 to 4.7 R_S and for the studied spacecraft orientations, the dominant current contributors are the $I_{e,c}$, I_i, $I_{ph,e}$ and $I_{se,e}$. The current balance is described by Equation 1. The $I_{e,h}$ is negligible due to the large ratio between the cold and hot electron densities. This ratio is decreasing for increasing radial distance from Saturn, beyond 4.6 R_S, and with increasing latitude. At 7.6 R_S, the $I_{e,h}$ is a significant current contributor. The current balance obtained for the spacecraft orientation and the environment at 7.6 R_S is given by Equation 2. The $I_{ph,c}$ and $I_{se,c}$ are negligible for all the studied cases, since the spacecraft is charged negatively and will repel the majority of the emitted photoelectrons and secondary electrons. Figure 9c shows that Cassini obtained a less negative surface potential at larger radial distance from Saturn. Eventually, outside of around 12.5 R_S, the spacecraft will charge positively (Livi et al., 2014).

This study also shows that a simplified spacecraft model, such as the one presented in Figure 1c, can be used without loosing accuracy in simulated parameters, such as plasma density and spacecraft potential. However, detailed simulations are needed in order to predict if a certain instrument, such as the Langmuir probe or CAPS, is located within the wake region at any given time. This is clearly illustrated in Figure 5, which shows the evolution of the wake around Cassini as the spacecraft is rolling and moving from 4.5 to 4.7 R_S. The results also show that detailed simulations are needed in order for a more accurate understanding and analysis of LP measurements.

Data Availability Statement

The Cassini 3D model is available at https://nasa3d.arc.nasa.gov/detail/jpl-vtad-cassini (2020-10-29). The Cassini ephemeris tool is available at http://www-pw.physics.uiowa.edu/∼jbg/cas.html (2020-10-29). The Cassini attitude tool is available at http://www-pw.physics.uiowa.edu/∼tfa/casatt.html (2020-10-29). The simulation software SPIS can be downloaded at https://www.spis.org/software/spis/get/ (2021-05-07). The RPWS/LP sweep data, which the ion density is obtained from is available on the Planetary Plasma

Interactions (PPI) node of NASA's Planetary Data System (PDS) at https://pds-ppi.igpp.ucla.edu/ in data set CO-SS_S-RPWS-3-LPUI-V1.0 (https://doi.org/10.17189/1519611, 2021-05-07). The Cassini RPWS/LP data are also available upon request at the University of Iowa and the Swedish Institute of Space Physics. Part of the ion density data set used in this article is also available on the Automated Multi-Data set Analysis (AMDA) tool at http://amda.cdpp.eu (2020-11-01), developed by the French Plasma Physics Data Center (CDPP) (http://www.cdpp.eu/). The LASP data set can be found on PDS/PPI in data set cassini-caps-fitted-parameters (https://doi.org/10.17189/1521149, 2021-05-07). The LANL moments are also on the PDS/PPI, in data set CO-S/SW-CAPS-5-DDR-ION-MOMENTS-V1.0 (https://doi.org/10.17189/1519609, 2021-05-07). The RPWS/electric field antenna electron density data are available at the PDS/PPI in the data set Cassini RPWS Electron Densities from Upper Hybrid and Plasma Wave Frequencies (2021-05-07). The MAG data can be found on the PDS/PPI in the data set CO-E_SW_J_S-MAG-3-RDR-FULL-RES-V2.0 (https://doi.org/10.17189/1521151, 2021-05-07).

Acknowledgments
The authors would like to thank Julie Webster, former manager of the Cassini Spacecraft Operations Office, for helpful discussions concerning the Cassini spacecraft model.

References

Arridge, C. S., McAndrews, H. J., Jackman, C. M., Forsyth, C., Walsh, A. P., Sittler, E. C., et al. (2009). Plasma electrons in Saturn's magnetotail: Structure, distribution and energization. *Planetary and Space Science*, *57*(14–15), 2032–2047. https://doi-org.insis.bib.cnrs.fr/10.1016/j.pss.2009.09.007

Elrod, M. K., Tseng, W.-L., Wilson, R. J., & Johnson, R. E. (2012). Seasonal variations in Saturn's plasma between the main rings and Enceladus. *Journal of Geophysical Research*, *117*, A03207. https://doi-org.insis.bib.cnrs.fr/10.1029/2011ja017332

Engwall, E., Eriksson, A. I., & Forest, J. (2006). Wake formation behind a positively charged spacecraft in flowing tenuous plasmas. *Physics of Plasmas*, *13*, 062904. https://doi-org.insis.bib.cnrs.fr/10.1063/1.2199207

Felici, M., Arridge, C. S., Wilson, R. J., Coates, A. J., Thomsen, M., & Reisenfeld, D. (2018). Survey of thermal plasma composition in Saturn's magnetosphere using Time-of-Flight data from Cassini/CAPS. *Journal of Geophysical Research: Space Physics*, *123*, 6494–6513. https://doi-org.insis.bib.cnrs.fr/10.1029/2017ja025085

Guillemant, S., Génot, V., Matéo Vélez, J.-M., Sarrailh, P., Hilgers, A., & Louarn, P. (2013). Simulation study of spacecraft electrostatic sheath changes with the heliocentric distances from 0.044 to 1 AU. *IEEE Transactions on Plasma Science*, *41*(12), 3338–3348. https://doi.org/10.1109/tps.2013.2246193

Gurnett, D. A., Kurth, W. S., Kirchner, D. L., Hospodarsky, G. B., Averkamp, T. F., Zarka, P., et al. (2004). The Cassini radio and plasma wave investigation. *Space Science Reviews*, *114*, 395–463. https://doi.org/10.1007/s11214-004-1434-0

Hadid, L. Z., Morooka, M. W., Wahlund, J.-E., Persoon, A. M., Andrews, D. J., Shebanits, O., et al. (2019). Saturn's ionosphere: Electron density altitude profiles and D-ring interaction from the Cassini Grand Finale. *Geophysical Research Letters*, *46*, 9362–9369. https://doi.org/10.1029/2018gl078004

Holmberg, M. K. G., Shebanits, O., Wahlund, J.-E., Morooka, M. W., Vigren, E., André, N., et al. (2017). Density structures, dynamics, and seasonal and solar cycle modulations of Saturn's inner plasma disk. *Journal of Geophysical Research: Space Physics*, *122*, 12258–12273. https://doi-org.insis.bib.cnrs.fr/10.1002/2017ja024311

Holmberg, M. K. G., Wahlund, J.-E., Morooka, M. W., & Persoon, A. M. (2012). Ion densities and velocities in the inner plasma torus of Saturn. *Planetary and Space Science*, *73*, 151–160. https://doi-org.insis.bib.cnrs.fr/10.1016/j.pss.2012.09.016

Lin, E. I., Stultzm, J. W., & Reeve, R. T. (1995). Test-derived effective emittance for Cassini MLI blankets and heat loss characteristics in the vicinity of seams, AIAA paper 95-2015, 30th AIAA Thermophysics Conference June 19-22.

Livi, R. J., Goldstein, J., Burch, J. L., Crary, F., Rymer, A. M., Mitchell, D. G., & Persoon, A. M. (2014). Multi-instrument analysis of plasma parameters in Saturn's equatorial, inner magnetosphere using corrections for spacecraft potential and penetrating background radiation. *Journal of Geophysical Research: Space Physics*, *119*, 3683–3707. https://doi-org.insis.bib.cnrs.fr/10.1002/2013ja019616

Miloch, W. J., Yaroshenko, V. V., Vladimirov, S. V., Pécseli, H. L., & Trulsen, J. (2012). Spacecraft charging in flowing plasmas; numerical simulations. *Journal of Physics: Conference Series*, *370*(1), 012004. https://doi.org/10.1088/1742-6596/370/1/012004

Morooka, M. W., Wahlund, J.-E., Andrews, D. J., Persoon, A. M., Ye, S.-Y., Kurth, W. S., et al. (2018). The dusty plasma disk around the Janus/Epimetheus ring. *Journal of Geophysical Research: Space Physics*, *123*, 4668–4678. https://doi-org.insis.bib.cnrs.fr/10.1002/2017ja024917

Morooka, M. W., Wahlund, J.-E., Hadid, L. Z., Eriksson, A. I., Edberg, N. J. T., Vigren, E., et al. (2019). Saturn's dusty ionosphere. *Journal of Geophysical Research Space Physics*, *124*, 1679–1697. https://doi-org.insis.bib.cnrs.fr/10.1029/2018ja026154

Pontius, D. H., & Hill, T. W. (2009). Plasma mass loading from the extended neutral gas torus of Enceladus as inferred from the observed plasma corotation lag. *Geophysical Research Letters*, *36*, L23103. https://doi.org/10.1029/2009gl041030

Sarrailh, P., Matéo-Vélez, J.-C., Hess, S. L. G., Roussel, J.-F., Thiébault, B., Forest, J., et al. (2015). SPIS 5: New modeling capabilities and methods for scientific missions. *IEEE Transactions on Plasma Science*, *43*(9), 2789–2798. https://doi-org.insis.bib.cnrs.fr/10.1109/tps.2015.2445384

Schippers, P., Blanc, M., André, N., Dandouras, I., Lewis, G. R., Gilbert, L. K., et al. (2008). Multi-instrument analysis of electron populations in Saturn's magnetosphere. *Journal of Geophysical Research*, *113*, A07208. https://doi.org/10.1029/2008ja013098

Schippers, P., Moncuquet, M., Meyer-Vernet, N., & Lecacheux, A. (2013). Core electron temperature and density in the innermost Saturn's magnetosphere from HF power spectra analysis on Cassini. *Journal of Geophysical Research: Space Physics*, *118*, 7170–7180. https://doi.org/10.1002/2013ja019199

Sittler, E. C., Andre, N., Blanc, M., Burger, M., Johnson, R. E., Coates, A., et al. (2008). Ion and neutral sources and sinks within Saturn's inner magnetosphere: Cassini results. *Planetary and Space Science*, *56*(1), 3–18. https://doi.org/10.1016/j.pss.2007.06.006

Sittler, Jr, E. C., Thomsen, M., Johnson, R. E., Hartle, R. E., Burger, M., Chornay, D., et al. (2006). Cassini observations of Saturn's inner plasmasphere: Saturn orbit insertion results. *Planetary and Space Science*, *54*(12), 1197–1210. https://doi.org/10.1016/j.pss.2006.05.038

Sjögren, A., Eriksson, A. I., & Cully, C. M. (2012). Simulation of potential measurements around a photoemitting spacecraft in a flowing plasma. *IEEE Transactions on Plasma Science*, *40*(4), 1257–1261. https://doi.org/10.1109/tps.2012.2186616

Thomsen, M. F., Reisenfeld, D. B., Delapp, D. M., Tokar, R. L., Young, D. T., Crary, F. J., et al. (2010). Survey of ion plasma parameters in Saturn's magnetosphere. *Journal of Geophysical Research*, *115*, A10220. https://doi.org/10.1029/2010ja015267

Wahlund, J.-E., André, M., Eriksson, A. I. E., Lundberg, M., Morooka, M. W., Shafiq, M., et al. (2009). Detection of dusty plasma near the E-ring of Saturn. *Planetary and Space Science*, *57*(14–15), 1795–1806. https://doi-org.insis.bib.cnrs.fr/10.1016/j.pss.2009.03.011

Wahlund, J.-E., Boström, R., Gustafsson, G., Gurnett, D. A., Kurth, W. S., Averkamp, T., et al. (2005). The inner magnetosphere of Saturn: Cassini RPWS cold plasma results from the first encounter. *Geophysical Research Letters*, *32*, L20S09. https://doi-org.insis.bib.cnrs.fr/10.1029/2005gl022699

Wang, X., Hsu, H.-W., & Horányi, M. (2015). Identification of when a Langmuir probe is in the sheath of a spacecraft: The effects of secondary electron emission from the probe. *Journal of Geophysical Research: Space Physics*, *120*, 2428–2437. https://doi-org.insis.bib.cnrs.fr/10.1002/2014ja020624

Wilson, R. J., Bagenal, F., Cassidy, T., Fleshman, B. L., & Crary, F. (2015). The relative proportions of water group ions in Saturn's inner magnetosphere: A preliminary study. *Journal of Geophysical Research: Space Physics*, *120*, 6624–6632. https://doi.org/10.1002/2014ja020557

Wilson, R. J., Bagenal, F., & Persoon, A. M. (2017). Survey of thermal plasma ions in Saturn's magnetosphere utilizing a forward model. *Journal of Geophysical Research: Space Physics*, *122*, 7256–7278. https://doi-org.insis.bib.cnrs.fr/10.1002/2017ja024117

Wilson, R. J., Tokar, R. L., & Henderson, M. G. (2009). Thermal ion flow in Saturn's inner magnetosphere measured by the Cassini plasma spectrometer: A signature of the Enceladus torus? *Geophysical Research Letters*, *36*, L23104. https://doi-org.insis.bib.cnrs.fr/10.1029/2009gl040225

Young, D. T., Berthelier, J.-J., Blanc, M., Burch, J. L., Bolton, S., Coates, A. J., et al. (2005). Composition and dynamics of plasma in Saturn's magnetosphere. *Science*, *307*(5713), 1262–1266. https://doi-org.insis.bib.cnrs.fr/10.1126/science.1106151

Young, D. T., Berthelier, J.-J., Blanc, M., Burch, J. L., Coates, A. J., Goldstein, R., et al. (2004). Cassini plasma spectrometer investigation. *Space Science Reviews*, *114*, 1–112. https://doi.org/10.1007/s11214-004-1406-4